Optimization of the optical properties of nanostructures through fast numerical approaches

François Thierry[a], Judikaël Le Rouzo[a], François Flory[a,b], Gérard Berginc[c], and Ludovic Escoubas[a]

[a]Aix-Marseille Université, Institut Matériaux Microélectronique Nanosciences de Provence-IM2NP, CNRS-UMR 7334, Domaine Universitaire de Saint-Jérôme, Service 231, 13397 Marseille, France;
[b]Ecole Centrale Marseille, 38 rue Joliot Curie, 13451 Marseille, France;
[c]THALES Optronique SA, 2 Avenue Gay Lussac, 78990 Elancourt, France

ABSTRACT

We present an improved and efficient numerical method to determine the optical properties of nanostructures starting from the electronic properties. We study the variation of electronic and optical properties induced by confinement effects in semiconductors quantum objects. We solve the time-independent Schrödinger equation with a new formulation of a shooting method under the effective mass approximation. This formulation is adapted to quantum wells, circular cross-section quantum wires and spherical quantum dots. We applied a correction on the mass to take into account the nonparabolicity of the band structure. The correction gives an accuracy comparable to more demanding calculation methods such as 8-bands k·p, tight binding or even semi-empirical pseudopotential methods. Our results remain valid even for low-bandgap materials and sizes as small as 1 nm. The calculation speed of our method allows optimization procedures that give better understanding of experimental results concerning CdS, CdSe, PbS and PbSe spherical quantum dots. We consider extensive data from the literature. We focus on the relations between the electronic structure and absorption and photoluminescence spectra measured on spin-coated PMMA thin-films containing (core)shell nanoparticles.

Keywords: quantum structures, EMA, nonparabolicity, CdSe, PbSe, coupled quantum wells, absorption, dielectric dipole approximation

1. INTRODUCTION

Changing the size, shape or composition of materials vary their electronic properties. The confinement effects in low-dimensional structures also change optical and electrical behaviors. The unique properties of nanostructured semiconductor materials have led to considerable interests from the optoelectronic community. In addition, recent progress in experimental formulation and numerical modeling have led to a growth of their use in various applications.[1]

Numerical studies give useful insights into the physical phenomena without delays or costs so that the association and sizing of materials can be optimized to design efficient devices, such as photovoltaic solar cells.[2] The optimization routines impose the numerical calculations to be fast and accurate. Speed and accuracy depend on the numerical method employed. Fast techniques often lack accuracy and exact ones demand too much computer resources.

The optical and electrical properties derive from the electronic ones,[1] so a precise evaluation of the confined energy levels is crucial. They are numerous models to study the size dependence of the energy levels due to spatial confinement.[3] The most simple ones derive from the particle-in-a-box (PIB) model.[4] Such methods like the effective mass approximation (EMA)[5] or quantum transfer matrix methods[6] are fast and give the general deviation from the bulk theory. They are generally valid for structures ranging from tenth of nanometers to several micrometers which is the size of electronics components. More precise models that take band mixing into account such as multi-bands k·p[7] or tight-binding (TB)[8] methods allow a more precise evaluation of the properties in the range of a few Angströms to hundreds of nanometers. Exact atomistic and ab-initio calculations such as

Nanophotonic Materials XI, edited by Stefano Cabrini, Gilles Lérondel, Adam M. Schwartzberg, Taleb Mokari,
Proc. of SPIE Vol. 9161, 916102 · © 2014 SPIE · CCC code: 0277-786X/14/$18 · doi: 10.1117/12.2061042

pseudopotential methods[9] and density functional theories (DFT)[10] are limited to the study of a few thousands atoms by hardware and computation time.

We adopt a rapid approach with the EMA that we solve using a shooting technique.[11] Speed, accuracy and stability are increased by developing the Schrödinger equation into a set of coupled differential equations that have less floating point operations.[12] Furthermore the usability is increased by a general formulation that can be applied to nanostructures of all dimensionality. We apply a correction on the effective mass with an energy dependence. The accuracy of the approach fit well with experimental data and more demanding methods such as 8x8 k·p, TB or SEPM.

In this study we present our method to calculate the energy levels of various nanostructures. We introduce some phenomenological aspects behind the nonparabolicity of the band structure to explain the sources of inaccuracies and the limits of the approach. We then study the limits of the current approach by confronting it to published results of the bandgaps of high- (CdS and CdSe) and low- (PbS and PbSe) bandgap semiconductor nanoparticles. The improvement given by the correction is demonstrated for an example of InGaAs/AlGaAs coupled quantum wells. We also give comparison between calculated electronic properties and measured absorption and photoluminescence of (CdSe)CdS colloidal quantum dots in PMMA matrix on glass substrate. We conclude on the perspective of extracting the effective permittivity of the films and of the quantum dots, the potential applications and the remaining points of improvement of the model.

2. DETERMINATION OF THE ELECTRONIC PROPERTIES

We consider a single charge in a steady state system. For speed consideration we have considered the effective mass approximation that contains the electrostatic interactions between the charges directly into the mass.

The EMA derive from the analytic dispersion relation for a free electron gas.[4] This PIB model approximates the band-structure around the gap to a parabola from which the curvature radius will condition the effective mass and energy level dispersion. The curvature at the extrema of this parabolic dispersion curve is expressed in the second derivative. A large curvature implies a large second derivative or a small radius of curvature that will lead to a small effective mass and vice-versa.

Actual band-structures show that the approximation by a parabolic shape is only valid for energies near the bands edge. The nonparabolicity of the bands is the main limit of the effective mass approximation and the main source of errors. It limits the resolution of the high-energies levels that are increasingly inaccurate the further away they are from the band edge. That is the reason why it is difficult to resolve the properties of low-bandgap materials under the EMA.[13] It is due to the domain of validity of the parabolic assumption that will be small in comparison to the actual band structure. Furthermore, the confinement effect that increases the energy level separation will lead to another limit of resolution for small sizes. We correct this problem by an effective mass that increases accordingly with the energy.

The correction[11] applies a parabolic increase to the effective mass that is conditioned by the energy difference from the band edge normalized by the amplitude of the bandgap to scale the effect. Thus each mass assigned to a position r in the structure will be corrected according to:

$$m^*(r,E) = m^*(r)\left[1 + \left(1 - \frac{m^*(r)}{m_e}\right)^2 \frac{E - V(r)}{E_g(r)}\right] \tag{1}$$

where $V(r)$ is the potential applied on the position. It should be noted that $E_g(r)$ increases also with the confinement. In our approach we use the bulk values only to calculate the first levels because they present the smallest deviations due to nonparabolicity. We then reuse the calculated values to determine the size-dependent gap to apply the nonparabolicity correction to higher levels.

We show an example of the nonparabolicity effect and the improvement given by the correction through the study of the conduction band of $Ga_{0.47}In_{0.53}As$ quantum wells in $Al_{0.48}In_{0.52}As$ barriers by comparing our results with those of Sirtori et al.[14] We have found that the results of our calculations are in perfect agreement with their experimental values with a maximum difference of 2 meV and that the nonparabolicity correction cannot be neglected under the effective mass approximation when considering energies that are of order or higher than

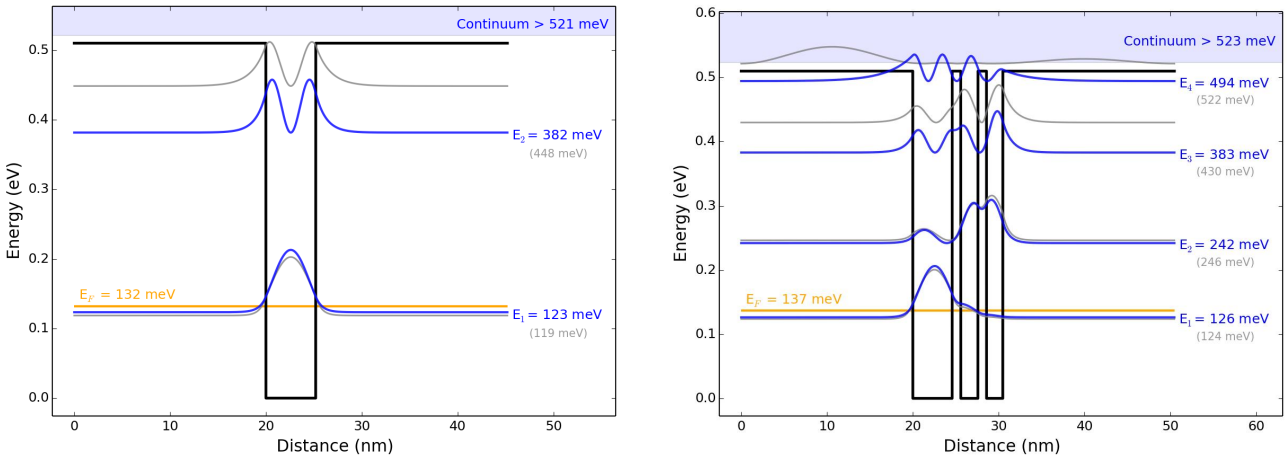

Figure 1. FIG. 3. Confined energy levels in the conduction band of the single-well and triple-well InGaAs/AlGaAs structures from Sirtori et al.[14] The thick blue lines are the results of our calculations, the thin grey lines are the results without the nonparabolicity correction. The Fermi level is also reported.

of the half-height of the confining potential. We emphasize that, with the correction, we retrieve the 8-bands k·p results of Sirtori and al. with a precision under 1 meV for a spatial resolution of $dr = 0.01$ nm.

We now present the numerical method to resolve the energies. The most common approach to solve the time-independent Schrödinger equation is to use finite difference and to calculate the eigenvalues and eigenfunctions of a tridiagonal matrix.[15] A faster technique,[16] although less employed in the semiconductor community, when using finite difference is the shooting technique.[17]

We use a shooting method implemented from Harrison's book.[11] We further improved the speed and stability by reformulating the shooting equation in a set of two coupled ones[12] that have less floating point operations. We formulated them so that it can be applied to both 2D, 1D and 0D quantum structures in a single formula (submitted for publication in Applied Physics Letters). The position is represented in scalar, cylindrical and spherical coordinates for quantum wells, wires and dots respectively. We solve for E the following coupled shooting equations:

$$\psi_{n,l}(r+dr) = \frac{rdrm^*(r)}{r+(N-1)m^*(r)}\tilde{\psi}_{n,l}(r) + \psi_{n,l}(r) \quad (2)$$

$$\tilde{\psi}_{n,l}(r+dr) = \frac{2dr}{\hbar^2}\left(V(r) + \frac{\hbar^2 l(l+N-2)}{2r^2m^*(r)} - E\right)\psi_{n,l}(r) + \tilde{\psi}_{n,l}(r) \quad (3)$$

The boundary conditions resulting from the continuity at interfaces condition are $\psi_{n,l}(\pm\infty) = 0$ and $\partial\psi_{n,l}(\pm\infty)/\partial r = 0$. $N = 3 - X$ is the dimensionality of an XD quantum structure ($X = 0$, 1 or 2), r is the position in m expressed in the correct coordinate system and $\psi_{n,l}$ is the radial part of the envelope of the wavefunction. We start the calculation at one end of the structures with the two first points of the shooting procedure equal to $\psi_{n,l}(0) = 0$ and $\tilde{\psi}_{n,l}(0) = 1$.

In 1D and 0D structures we should to start the evaluation of the energy levels from the middle of the structures with $\psi_{n,l}(0) = 1$ and $\tilde{\psi}_{n,l}(0) = 1$ as starting values. But to allow the study of laterally coupled structures and to have common starting values for all dimensions we used the fact that, as the EMA derives from the PIB model, ΔE depends linearly on S/D^2, the inverse of the square diameter or length.[18] The slopes S are 1.0,[19] 1.17[20] and 2.0[21] for wells, wires and dots respectively. We verified that we retrieve the same results between the calculations starting from the middle of the structure and the ones starting at one end for which we multiplied the corresponding energy by the appropriate slope. The calculation of coupled 1D and 0D quantum structures is only valid if running along the axis that goes to all the centers of symmetry.

The implementation of this method is straightforward. It allows the quick evaluation of electronic properties of most nanostructures and should be of interest to many scientific studies covering a wide spectrum of applications.

All our code is written in Python except for the core equations that are implemented in Cython for speed. The wavefunction envelopes calculated with this method have to be normalized according to $\psi(r) \rightarrow \psi(r)/\sqrt{\int \psi^2(r)dr}$ to be quantitatively compared in models like the electrostatic dipole approximation that serves to determine optical properties of nanostructures.

To study the capability of our approach we study the size-confinement of the bandgap for colloidal quantum dots that present the highest confinement. We model the quantum dots with finite potential as nanospheres of a certain dimension comprise between vacuum domains of same sizes. We fixed the band offsets between the materials and the vacuum. This allows the results to become more independent of the matrix and therefore allows the comparison of data from different sources. We use the values of the electronic affinity χ_A as band offset in the conduction band. In the valence band, we use $\chi_A + E_g$. This allows the method to be more accurate and to compare the calculation with arbitrary absorption data. The Brus equation[21] corrects the PIB model of spherical geometries through a screening term that describes electrostatic forces. It is often reported as a first approximation in publications concerning quantum dots because it extends the validity range of the PIB model while keeping the speed of resolution and retaining the simplicity. Kayanuma further improved this formulation by accounting spatial correlation between the charges with the effective Rydberg energy.[22]

We corroborated our results with exhaustive bandgaps data from the literature and found excellent agreement between experimental results and more accurate methods that take band mixing into account and therefore are not subject to the nonparabolicity limitation. In figure 2 we present the results of our calculation for CdSe and PbS QDs with (solid line) and without (dashed line) the correction. We see that, as expected, in both cases the Brus equation diverges when the confinement is to strong, that is, for small sizes and low-bandgap. We obtain excellent agreement with experimental data and more precise but more demanding methods.

This approach has been validated through the study of the bandgaps of quantum dots of various semiconductors. We fit the absorption data with a sizing curve of the form $E_g(D) = E_g + 1/(aD^2 + bD + c)$. The comparison of our results with the fit allows us to estimate the accuracy of our method in comparison with other parameters such as bulk bandgaps and sizes. The figure 3 presents the deviation in eV between of our results with the correction and the sizing curve for the semiconductors of this study. We consider 100 sizes ranging from 0.5 nm to 20 nm. This test depends heavily on the quality of the fit, the more there are data points better is the fit. We can see that the results for CdS present the higher deviation, this is due to the lack of data points that give an inaccurate fit. Nonetheless we find that the mean deviation under 100 meV is around 15 meV, that corresponds to a shift of $\approx$ 5 nm when comparing to experimental spectra from optical measurements. Also this is a fit on data from different sources that where in different matrices, caped with different ligands,... That changes the electronic affinity, the confinement potential and thus the energy levels that are calculated. Comparisons

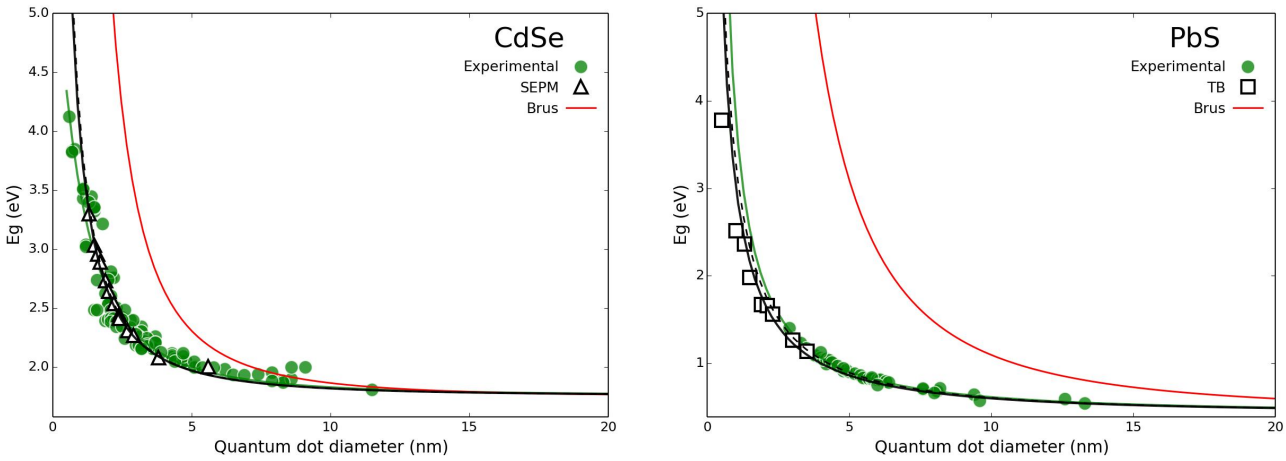

Figure 2. Calculation of the bandgap variation of high- and low-bandgap CdSe and PbS nanospheres. Comparison with experimental data and semi-empirical pseudopotential (SEPM) and tight-binding (TB) calculations from the literature. Results with Brus equation are also shown.

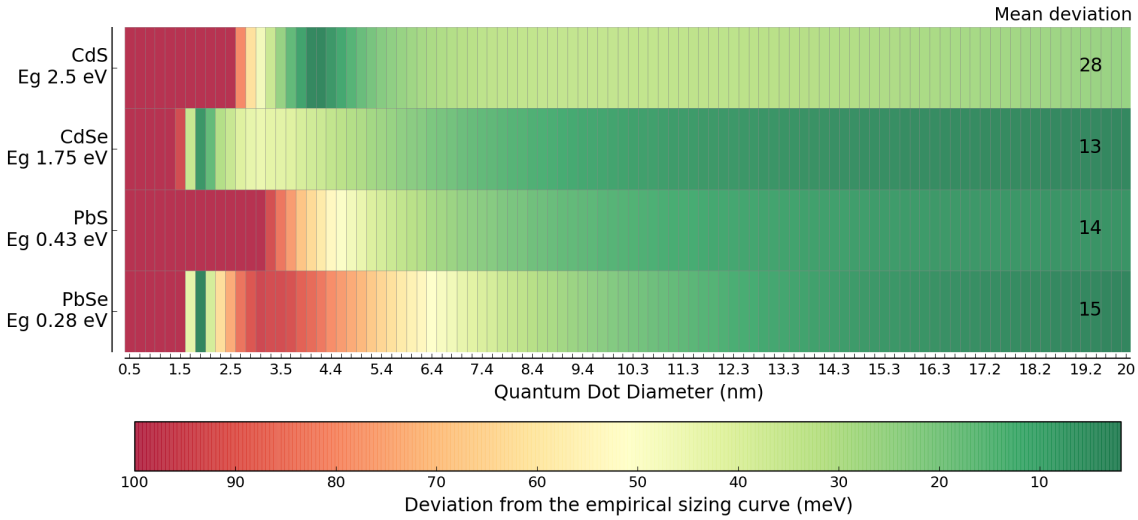

Figure 3. Test of the capability of the method to determine the confined bandgap of different semiconductors.

with experimental samples need a more careful study on those aspects. We also observe the deterioration of the resolution for decreasingly low-bandgap materials.

3. QUANTUM DOTS IN PMMA THIN-FILMS

To study the optical properties of quantum dots (QDs) we realized thin-films of (core)shell (CdSe)ZnS, (CdSe)CdS structures and PbS nanoparticles. We choose a PMMA matrix because of its ease of use and its transparency in the visible spectrum. The (CdSe)ZnS dots are of seven sizes ranging from 2.5 to 6.7 $\pm$ 0.5 nm core diameters with shells of 0.6 $\pm$ 0.1 nm. They were bought from Plasmachem. The (CdSe)CdS and PbS nanospheres were synthesized by the cole suprieure de physique et de chimie industrielle (ESPCI) in Paris. We dispersed the dots in chloroform and mixed it with PMMA in solution with a 10% concentration in mass. We then made the films by spin-coating.[23] We optimized deposition time and rotation speed to have the most uniform layer. We found that optimum results when performing optical measurement were obtained for films deposited at 2000-2500 rpm for 20 sec. We further flattened the samples surfaces by annealing in oven at 120°C for 15 minutes.

We evaluated the thicknesses by measuring step-differences with an optical profilometer and found that the layers that we made have a thickness of around 1 micron. We obtained the absorption, transmission and reflectance of our samples with an integrating sphere in the visible. We also used a spectrophotometer to obtain absorption spectra with better resolution and measured room-temperature photoluminescence to study the resulting spectra. We currently started ellipsometry measurements to extract the refractive index.

The figure 4 presents absorption and photoluminescence spectra of the (CdSe)CdS QDs. The positions of the peaks that are the electronic transitions are extracted using the first derivative to compare with our numerical results. The mean diameter of the CdSe core estimated from the TEM images reported on the figure is 5.3 nm with a CdS shell of around 0.5 nm.

4. OPTICAL PROPERTIES: DIELECTRIC DIPOLE APPROXIMATION

Once we have the energy levels we perform carriers statistics evaluation. We determine the intrinsic charge density of each band. We calculate the Fermi energy E_F and levels population N_i at 0K. For other temperatures we integrate the Fermi-Dirac distribution and resolve the populations. This allows us to discriminate the empty levels. To extract the material properties we consider the transitions between levels as dielectric oscillators. Under the dielectric dipole approximation, the oscillator strength of a transition from a level i to a level j reads

$$f_{ij} = \frac{2m^*}{\hbar^2} \Delta E_{ji} |M_{ij}|^2, \tag{4}$$

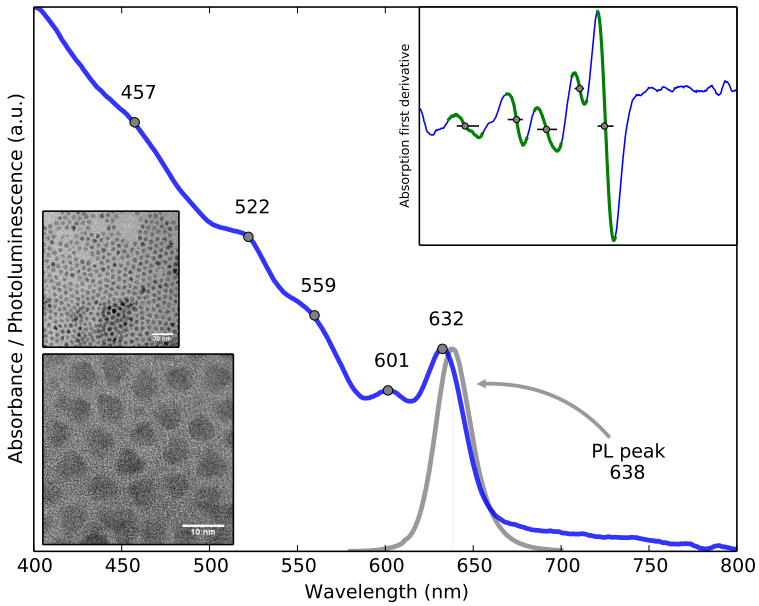

Figure 4. Absorption and photoluminescence spectra of (core)shell (CdSe)CdS quantum dots. Peak positions are determined from the first derivative. Sizes are determined from the TEM pictures (ESPCI measurements).

where the energetic difference ΔE_{ji} gives the spectral position of the transition, that is, the position of a peak on absorption or photoluminescence spectra. M_{ij} is the dipole matrix element corresponding to the overlap integral of the wavefunctions. It gives the amplitude of the transition. Attention have to be paid to the fact that this formulation is not adapted to heterostructures because the mass m^* does not reflect the distribution probability of the charge in the structure. We calculate the effective mass specific to each level by normalizing it to the shape of the wavefunction:[24]

$$m_i^* = 1/\int \frac{|\psi_i|^2}{m^*(r)} dr \tag{5}$$

Now that we have the electronic properties and transitions characteristics we simulate the absorption starting from the Fermi golden rule. The absorption coefficient for a particular transition $i \to j$ reads:[25]

$$\alpha_{ij}(\hbar\omega) = \hbar\omega \frac{16\pi^2 \beta_{FS} \Delta N_{ji}}{\sqrt{\epsilon_r} V_{conf}} |M_{ij}|^2 d(\Delta E_{ji} - \hbar\omega) \tag{6}$$

β_{FS} is the fine-structure constant, ΔN_{ji} is the population difference between the levels, ϵ_r is the relative permittivity and V_{conf} is the confinement volume that is occupied by the wavefunctions. The function $d(\Delta E_{ji} - \hbar\omega)$ represents the absorption peak under the form of a Lorentzian of arbitrary width Γ fixed to 10 meV.

$$d(\Delta E_{ji} - \hbar\omega) = \frac{1}{\pi} \left[\frac{\hbar\Gamma}{(\hbar\omega - \Delta E_{ji})^2 + (\hbar\Gamma)^2} \right] \tag{7}$$

The sum of the absorptions of all the transitions give the simulated spectrum. The main broadening mechanism in the optical properties of solution-processed quantum dots is the size dispersion. We can model it by a log-normed function $h(d, d_0, \sigma)$[26] that we multiply with d

$$h(d, d_0, \sigma) = \frac{1}{\sqrt{2\pi}} \frac{1}{d} \frac{1}{\ln \sigma} \exp \left[-\frac{1}{2} \frac{\ln^2(d/d_0)}{\ln^2 \sigma} \right] \tag{8}$$

d and d_0 are particle and mean diameters respectively and σ is the standard deviation of the distribution. This equation can either serve to model or fit an experimental distribution.

To describe photoluminescence (PL) one must know the exciton binding energy that represents the separation between the firsts absorption and PL peaks, often called Stocke shift. We use a formulation developed by Hanken in 1956

$$E_b = -\frac{2e^2}{4\pi\epsilon_r\epsilon_0}\int_0^{r_e}\psi_{0,1}^2(r_h)r_h dr_h \int_0^{r_h}\psi_{0,1}^2(r_e)r_e^2 dr_e \tag{9}$$

The photoluminescence can then be evaluated in the same manner than presented here for absorption[26] using the transitions that are related to the exciton, donor and acceptor levels.

Another important property that appears throughout this section is the dielectric permittivity that changes with confinement due to the shifts of the energy levels. A first approximation of the size dependence of the permittivity, originally developed by Hanken, readapted later reads:

$$\frac{1}{\epsilon_r(d)} = \frac{1}{\epsilon_\infty} - \left[\frac{1}{\epsilon_\infty} - \frac{1}{\epsilon_0}\right]\left[1 - \frac{\exp(-d/\rho_e) + \exp(-d/\rho_h)}{2}\right] \qquad \rho_{e,h} = \left(\frac{\hbar}{2m_{e,h}^*\omega_{LO}}\right)^{1/2} \tag{10}$$

We can then use this correction to estimate the overall permittivity[27]

$$\epsilon(\omega) = \epsilon_r(d) + \omega_p^2 \sum_i \sum_j \frac{f_{ij}}{\omega_{ij}^2 - \omega^2 - i\gamma\omega} \tag{11}$$

5. CONCLUSION

The EMA method presented in this paper can be applied to quantum wells, wires and dots structures. Our formulation is simple yet accurate, easy to implement and performs in few microseconds on a particular structure. We highlighted the limiting cases of narrow bandgap materials or energies that are far away from the bands edges that we explained with phenomenological considerations. Those limitations have been corrected by transforming the effective mass to be energy-dependent in order to account the nonparabolicity of the band structure. We provide examples of bandgap calculations obtained with our approach that compare well with published work on CdS, CdSe, PbS and PbSe quantum dots. We have considered only a few examples but the method gives accurate results on a wide range of materials given the appropriate input parameters. The rapidity of our method allows to experiment with physical parameters when comparing to experimental results in order to deepen our understanding of the samples and the physical phenomena in place. The methodology to calculate the absorption spectra and the permittivity from the electronic properties is presented. Further work about the determination of electronic and optical properties of quantum dot materials solar cells using our technique will be carried out.

ACKNOWLEDGMENTS

We thank Dr. Emmanuel Lhuillier from the ESPCI for providing us the (CdSe)CdS and PbS dots.

REFERENCES

1. Flory, F., Escoubas, L., and Berginc, G., "Optical properties of nanostructured materials: a review," *Journal of Nanophotonics* **5**(1), 052502 (2011).
2. Nozik, A. J., "Nanoscience and nanostructures for photovoltaics and solar fuels," *Nano Letters* **10**(8), 2735–2741 (2010).
3. Saad, Y., Chelikowsky, J. R., and Shontz, S. M., "Numerical methods for electronic structure calculations of materials," *SIAM Review* **52**(1), 3–54 (2010).
4. Kittel, C., [*Physique de l'état solide: cours et problèmes*], Sciences sup, Dunod (2005).
5. Sham, L. J. and Nakayama, M., "Effective-mass approximation in the presence of an interface," *Physical Review B* **20**(2), 734–747 (1979).

6. Jonsson, B. and Eng, S. T., "Solving the schrodinger equation in arbitrary quantum-well potential profiles using the transfer matrix method," *IEEE Journal of Quantum Electronics* **26**(11), 2025–2035 (1990).
7. Voon, L. and Willatzen, M., [*The k p Method: Electronic Properties of Semiconductors*], Springer (2009).
8. Goringe, C. M., Bowler, D. R., and Hernndez, E., "Tight-binding modelling of materials," *Reports on Progress in Physics* **60**(12), 1447–1512 (1999).
9. Andrae, D., Huermann, U., Dolg, M., Stoll, H., and Preu, H., "Energy-adjusted ab-initio pseudopotentials for the second and third row transition elements," *Theoretica chimica acta* **77**(2), 123–141 (1990).
10. Geerlings, P., De Proft, F., and Langenaeker, W., "Conceptual density functional theory.," *Chemical reviews* **103**(5), 1793–1873 (2003).
11. Harrison, P., [*Quantum Wells, Wires and Dots: Theoretical and Computational Physics of Semiconductor Nanostructures*], Wiley (2005).
12. Paul, S. F.-P. and Fouckhardt, H., "An improved shooting approach for solving the time-independent Schrödinger equation for III/V QW structures," *Physics Letters A* **286**, 199–204 (2001).
13. Pellegrini, G., Mattei, G., and Mazzoldi, P., "Finite depth square well model: Applicability and limitations," *Journal of Applied Physics* **97**(7) (2005).
14. Sirtori, C., Capasso, F., Faist, J., and Scandolo, S., "Nonparabolicity and a sum rule associated with bound-to-bound and bound-to-continuum intersubband transitions in quantum wells," *Physical Review B* **50**(12), 8663–8674 (1994).
15. Cooney, P. J., Kanter, E. P., and Vager, Z., "Convenient numerical technique for solving the one-dimensional schrödinger equation for bound states," *American Journal of Physics* **49**(1), 76–77 (1981).
16. Killingbeck, J., [*Microcomputer Algorithms: Action from Algebra*], Adam Hilger (1991).
17. Stoer, J. and Bulirsch, R., [*Introduction to Numerical Analysis*], Texts in Applied Mathematics, Springer (2002).
18. Yoffe, A. D., "Semiconductor quantum dots and related systems: Electronic, optical, luminescence and related properties of low dimensional systems," *Advances in Physics* **50**(1), 1–208 (2001).
19. Dingle, R., [*Confined Carrier Quantum States in Ultrathin Semiconductor Heterostructures*], 21–48, Springer Berlin Heidelberg (1975).
20. Nanda, K. K., Kruis, F. E., and Fissan, H., "Energy levels in embedded semiconductor nanoparticles and nanowires," *Nano Letters* **1**(11), 605–611 (2001).
21. Brus, L. E., "Electron electron and electron hole interactions in small semiconductor crystallites: The size dependence of the lowest excited electronic state," *The Journal of Chemical Physics* **80**(9) (1984).
22. Kayanuma, Y., "Quantum-size effects of interacting electrons and holes in semiconductor microcrystals with spherical shape," *Phys. Rev. B* **38**, 9797–9805 (Nov 1988).
23. Lin, H.-J., Vedraine, S., Le-Rouzo, J., Chen, S.-H., Flory, F., and Lee, C.-C., "Optical properties of quantum dots layers: Application to photovoltaic solar cells," *Solar Energy Materials and Solar Cells* **117**, 652–656 (2013).
24. Kosti, R. and Stojanovi, D., "Nonlinear absorption spectra for intersubband transitions of cdse/zns spherical quantum dots," *Journal of Nanophotonics* **5**(1), 051810–051810–9 (2011).
25. Tas;, H. and Sahin, M., "The inter-sublevel optical properties of a spherical quantum dot-quantum well with and without a donor impurity," *Journal of Applied Physics* **112**(5), 053717 (2012).
26. Semaltianos, N. G., Logothetidis, S., Perrie, W., Romani, S., Potter, R. J., Sharp, M., French, P., Dearden, G., and Watkins, K. G., "Cdse nanoparticles synthesized by laser ablation," *EPL (Europhysics Letters)* **84**(4), 47001 (2008).
27. Scholl, J. A., Koh, A. L., and Dionne, J. A., "Quantum plasmon resonances of individual metallic nanoparticles," *Nature* **483**(7390), 421–427 (2012).